Purification and Analysis of WT Uricase

Heather MacGregor* and Alexandria Taylor

University of California, Santa Barbara

Abstract: Urate oxidase (uricase, UOx, EC 1.7.3.3) catalyzes the O_2 degradadation of UA into 5-hydroxyisourate, the first step in a pathway leading to allantoin, an easily-excretable substance 5-10× more soluble than UA.[1] Although UOx is an endogenous enzyme found in most mammals, it is inactivated in humans. However, recombinant UOx species, such as Rasburicase, have shown to be promising candidates for the treatment of diseases including hyperuricemia and tumor lysis syndrome. However, uricase tends to form aggregates in solution that are highly immunogenic. Previously, XL-1-Blue Supercompetent *E. coli* were transformed with plasmids containing the sequences for C319* and C319*-C253R mutants of *Bacillus subtilis* UOx. These mutants were designed in order to prevent this phenomenon of aggregation. Here, the wild-type enzyme is purified from the cell lysate of BL21 Competent *E. coli* cells. The purified WT enzyme will be used as a baseline for kinetic and light-scattering studies of the recombinant mutants.

Keywords: Plasmid

1 Introduction and Background

Tumor lysis syndrome (TLS) is a potentially lethal complication of aggressive cancer treatment, which causes massive tumor cell lysis and a corresponding release of purine metabolites into the circulatory system. These metabolites are rapidly converted by hepatic xanthine oxidase to uric acid (UA), leading to hyperuricaemia. As a consequence, urine becomes supersaturated with UA and crystals of UA precipitate in the renal tubules and distal collecting system, which ultimately results in acute renal failure.
Antihyperuricemic therapy may be applied as a preventative measure in patients at intermediate to high risk for TLS or as a treatment for TLS-associated hyperuricemia. Before 2002, antihyperuricemic therapy was limited to allopurinol, a xanthine oxidase inhibitor that has serious side effects when administered at effective doses.[2,3,4] Rasburicase, a recombinant urate oxidase (rUOx), was approved by the US Food and Drug Administration for children in 2002 and adults in 2009.[5] Although both drugs aim to control uric acid levels by interfering with purine catabolism (see Fig. 1), their mechanistic differences highlight an important distinction from a clinical efficacy standpoint: both agents prevent the accumulation of UA, but only rasburicase treatment enables the breakdown and excretion of pre-existing UA.

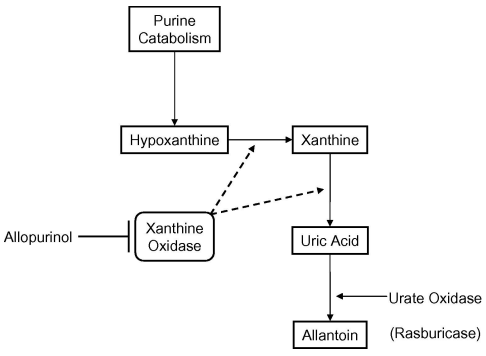

Fig. 1: Mechanism of action: rasburicase and allopurinol.[6]

Rasburicase is a recombinant form of *Aspergillus flavus* urate oxidase (uricase, UOx, EC 1.7.3.3), an enzyme that catalyzes the O_2 degradadation of UA into 5-hydroxyisourate,[7] the first step in a pathway leading to allantoin, an easily-excretable substance 5-10× more soluble than UA.[1] Although UOx is an endogenous enzyme found in most mammals, it is inactivated in humans as a result of two nonsense mutations that occured during evolution.[8] The active enzyme is a tunnel-shaped homo-tetramer[9] composed of four identical 34 kDa subunits.[10] Each of the four active sites is formed at the subunit-subunit interface (see Fig. **??**B).
Rasburicase has been shown to be significantly more effective than allopurinol in the treatment of hyperuricemia and was associated with significantly shorter ICU and overall hospital stays and lower total inpatient costs.[11,12] Unfortunately, the storage and application of aqueous rUOX has been hindered by its immunogenicity and lack of stability, especially with increased temperature and concentration.[13] Immunogenicity is caused by a wide variety of factors, but the propensity of protein aggregation is currently considered one of the highest risk factors for drug immunogenicity.[14] Tetrameric UOx has a high tendency to aggregate to form octomers or larger aggregates, which are highly immunogenic.

* E-mail address: macgregor@ucsb.edu doi: 10.1000/999

Aggregation of UOx can be brought about by several mechanisms that have, thus far, been discussed in the literature. The first proposed mechanism is that the dissociation of the UOx tetramer leads to transient monomers with a high ratio of solvent-exposed hydrophobic residues, and these transient structures are more prone to aggregation and, eventually, precipitation.[15] Thus, the lack of stability in the overall tetrameric structure of UOx is responsible for its propensity to aggregate. This mechanism is supported by results of a recent study showing that disruption between interactions at the subunit-subunit interface leads to the inactivation and aggregation of UOx, and that this inactivation can be prevented by addition of glycerol and/or trimethylamine oxide, which act to stabilize hydrophobic interactions and backbone structure, respectively.[16,17] However, the concentration-dependent instability is not due to subunit dissociation.[18] Additionally, a more recent finding suggests that interactions between the flexible C-terminal loop and the residues of a neighboring subunit are required for the stability of the tetramer.[19]
A second, although not contradictory, proposal attributes aggregation to the formation of disulfide bonds between tetramers.[20] Aggregation caused by this effect can be largely prevented by the addition of 1-5 mM of the reducing agent dithiothreitol in the laboratory settings, although such conditions are unsuitable for medical applications. Each UOx tetramer contains a single surface-accessible cysteine residue: C253 for *Bacillus subtilis* UOx. This residue was previously validated as a target for mutagenesis and a C249S mutant of *Candida* UOx displayed reduced aggregation in comparison to the WT enzyme.[20]
We previously successfully transformed XL-1-Blue Supercompetent *E. coli* colonies with plasmids containing the sequences for C319* and C319*-C253R mutants of *Bacillus subtilis* UOx. Here, we present our purification of the wild-type enzyme from the cell paste of induced BL21 Competent *E. coli* cells. The purified WT enzyme will be used as a baseline in kinetic and light-scattering studies of the recombinant enzymes.

2 Methods

2.1 Protein Expression

BL21 Competent *E. coli* (New England BioLabs, Inc.) were transformed with a pET-14b plasmid (Novagen), a T7 promoter-based expression vector, containing the sequence for wild-type *B. subtilis* UOx containing a 6xHis-tag. Instructions from the manufacturer were followed to induce large-scale protein expression; after IPTG induction, protein was expressed overnight at 25 °C.[21,22] Induced cells were pelleted by centrifugation at 5,000 rpm for 15m at 4 °C. Cell paste (ca. 3 grams per liter) was stored at –80 °C[1]. An aliquot containing 665.3 mg of cell paste was used for the purification.

2.2 Preparation and Clarification of the Cell Extract

Cells were resuspended in lysis buffer and incubated for 10m at room temperature while mixing. After addition of 2 mM DTT, the cell lysate was incubated on ice for 20m. To minimize foaming, 2 μL Antifoam 204 0.1% (*v/v*) was added to the lysis solution. The sample was sonicated (duty cycle 50%; output control 4) 4 × 30s with 1m intervals between each sonication. After transferring the lysate to a 30 mL centrifuge tube, cellular debris was pelleted by centrifugation at 9,000 rpm for 10m and discarded. Nucleic acids were precipitated by addition of 60 μL protamine sulfate (50 mg/mL), and insoluble nucleic acid-protamine sulfate complexes were pelleted by centrifugation at maximum speed for 6m and discarded. To selectively precipitate UOx, ammonium sulfate (crystalline) was added to achieve 60–65% saturation and incubated at -20 °C for 1 week. UOx was pelleted by centrifugation at 12,000 rpm for 7m. However, the pellet floated to the top of the solution; this phenomenon appears to be common for ammonium sulfate precipitates.[23] The floating pellet was redissolved and pelleted again at maximum speed in the microcentrifuge.

2.3 Dialysis

The protein pellet was redissolved in cold Buffer A and dialyzed against Buffer A overnight in a 3 mL-capacity Slide-A-Lyzer™ Dialysis Cassette (ThermoFisher Scientific) attached to a float buoy while stirring at a slow speed.

2.4 Nickel Affinity Column Chromatography

A glass Econo-Column® Chromatography Column, 10 cm (Bio-Rad Laboratories, Inc.) was packed with 6 mL of 50% Ni-NTA affinity resin (QIAGEN Ni-NTA Agarose) and pre-equilibrated with cold Buffer A at 0.75 mL/min using a Model EP-1 Econo Pump (Bio-Rad Laboratories, Inc.). After dialysis, the cytoplasmic extract was spun at maximum speed for 10m and chilled on ice before loading directly into the column at 0.5 mL/min. The column was washed with cold Buffer A. About 20 mL of the initial flow-through was collected and tested for UV absorbance at 280 nm and UOx activity. Next, the column was washed with 25 mL of cold Buffer B at 1.0 mL/min until the absorbance of the eluant at 280 nm returned to baseline. Buffers B (40 mM imidazole) and C (500 mM imidazole) were added to the inner and outer compartments, respectively, of a gradient former (Life Technologies/GibcoBRL). While stirring Buffer B at moderate speed, the gradient former was connected to the inlet tube of the pump, and the column was eluted at 1.0 mL/min into 2 mL receptacle tubes.

2.5 SDS Polyacrylamide Gel Electrophoresis

Gels were prepared using a Mini-PROTEAN® Tetra Handcast System, spacer plates with 0.75 mm integrated spacers and 15-well comb, 20 μl (Bio-Rad Laboratories, Inc.). Gels were cast according to the instructions provided by the manufacturer;[24,25] however, the stacking gel was poured to 5 mm below the comb to account for the high salt concentration of the samples. Samples were mixed

[1]Protein expression was performed by the instructor.

with 4X Loading Dye at a 1:2 volumetric ratio, incubated at 95 °C for 5m in a T100™ Thermal Cycler (Bio-Rad Laboratories, Inc.), then spun at maximum speed for 2m to pellet insoluble material. Marker proteins and samples were loaded into wells as seen in Table 4 using 0.5-10 μL micropipette tips[2]. Two gels were run together at 200 V for 35m. Gels were stained using a 0.025% Coomassie Blue R-250 staining solution, soaked in destaining solution overnight, and imaged on top of a white light illumination box with an iPhone 7 Plus Dual 12MP rear camera (Apple, Inc.). If necessary, gels were stored in gel storage solution before discarding.

2.6 Concentration and Buffer Exchange

Fractions with the highest activity were pooled together and dialyzed against 50 mM Tris, pH 8.0 with 2 mM DTT overnight. An aliquot of the dialysate was concentrated 5× by ultrafiltration to a volume of 100 μL using an Ultra-0.5 Centrifugal Filter Tube (Amicon).

2.7 Activity Assay

Because urate oxidase catalyzes the degradation of uric acid, enzyme activity over the course of the purification protocol can be monitored by monitoring the decrease in absorbance of the substrate, urate, at 292 nm; this is proportional to the activity of the enzyme.[26] However, because the product of this reaction absorbs at the same wavelength, this assay is expected to underestimate the true rate of urate disappearance.[27] Thus, assays were performed at an elevated pH Working at elevated pH can minimize interference from 5-hydroxyisourate.[28] Urate solutions in 70 mM CHES (pH 9.15–9.25) were prepared fresh daily from stock solution (0.2 M) to approximately 100 μM, and their exact concentrations were determined spectrophotometrically ($\varepsilon_{292} \approx 12{,}300$ cm^{-1} M^{-1}).[7] Activity assays were performed by monitoring the absorbance at 292 nm of solutions of protein sample (aliquoted at each stage of the purification) in about 100μM of the substrate for 60s.

2.8 Bradford Assay

The crude cell lysate was dissolved 20-, 40-, and 80-fold in 40 mM Tris-HCl, pH 8.0 and the absorbance values at 260 and 280 nm were recorded in a quartz cuvette with a UV-Vis spectrophotometer (Shimadzu BioSpec 1601). A rough estimate of the total protein concentration (with corrections for nucleic acid contamination) was calculated according to:

$$\text{Total Protein Concentration (mg/ml)} = (1.55 \times A_{280}) - (0.76 \times A_{260}) \tag{1}$$

An appropriate amount of concentrated Bradford Dye Reagent (Bio-Rad Laboratories, Inc.) was diluted in distilled water on the day of use. Standard BSA solutions were serially diluted from a freshly prepared BSA stock solution and mixed throuroughly with diluted Bradford Dye Reagent (1:50) in a plastic cuvette and incubated at room temperature for 15m. After baselining with Bradford Dye Reagent in water, the absorbance at 595 nm of each standard solution was measured.
The absorbance at 595 nm for each aliquot stored over the course of the purification process was obtained in the same fashion as above. Based on the A_{280} assay, aliquots were diluted 80-fold prior to mixing with Bradford Dye Reagent to keep the total protein content within the linear range of the Bradford assay.[22,29] A calibration curve for the assay was obtained by performing linear regression on the standard dataset in Wolfram Mathematica and used to determine the total protein content in each aliquot based on the observed A_{595}.

3 Results

3.1 Activity Assays

The observed rate values, activities, and specific activities from aliquots taken from various stages in the protein purification are listed in Table 1. After protamine sulfate treatment, the observed rate of substrate degradation was 0.0015 AU/min.

Tab. 1: Activity assay results throughout the process of purification of 665.3 mg of cell paste.

Step	Volume (mL)	Enzyme (mg/mL)	Rate (AU/min)	Activity (U/mL)	Specific Activity (U/mg)	Yield (%)
Crude cell lysate	16	1.90325385	-0.2673042	0.54330122	0.285459146	100.00
Precipitation with protamine sulfate	16	2.01130154	-0.2083032	0.423380488	0.210500753	73.74
Redissolved $(NH_4)_2SO_4$ pellet	17	1.945479384	-0.3971143	0.807142886	0.414881233	145.34
Dialyzed $(NH_4)_2SO_4$ pellet	3.0	2.057252856	-0.4023	0.817682927	0.397463503	139.24
Chromatography (pooled)	9.0	0.355812221	-0.01	0.081300813	0.228493594	80.04
Dialysis	3.5	0.27226861	-0.0075	0.076219512	0.279942341	98.07
Concentrated (Final preparation)	0.1	0.188725	-0.131	2.662601626	14.10836734	4942.34

3.2 Bradford Assay

The BSA standard dataset (Table 7) was plotted with [BSA] (mg/mL) on the x-axis and A_{BSA} on the y-axis. Linear regression found the line of best fit to be:

$$A = 0.0200483 + 0.800632\gamma \qquad (R^2 = 0.998374) \tag{2}$$

[2]No gel-loading tips were available at the time.

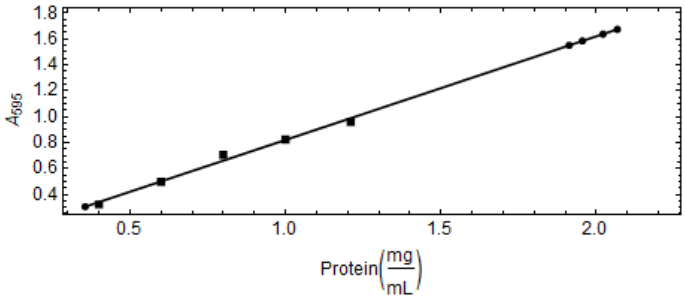

Fig. 2: Bradford Assay BSA standard plot with line of best fit. (BSA standards = ●; sample data = ■).

where γ is the concentration of protein in the sample. From this relationship, we were able to derive the protein concentration in each aliquot (Table 1) from its absorbance at 595 nm.

3.3 Nickel Affinity Column Chromatography

The column flow-through had an A_{280} of 2.9745 and displayed some enzymatic activity; its observed rate of substrate degradation was 0.1101 AU/min. The wash-through also displayed some enzymatic activity; its observed rate was 0.1449 AU/min. Some issues arose in this portion of the experiment that resulted in severe eluant leakage onto the bench as well as the failure to obtain a linear gradient of imidazole flowing through the column, improperly fast flow rates. Some instances occured where the top of the packed resin became dry. The rates of substrate degradation for each fraction are shown in Fig. 3. Fractions 7-12 displayed the greatest enzymatic activity and were thus pooled together.

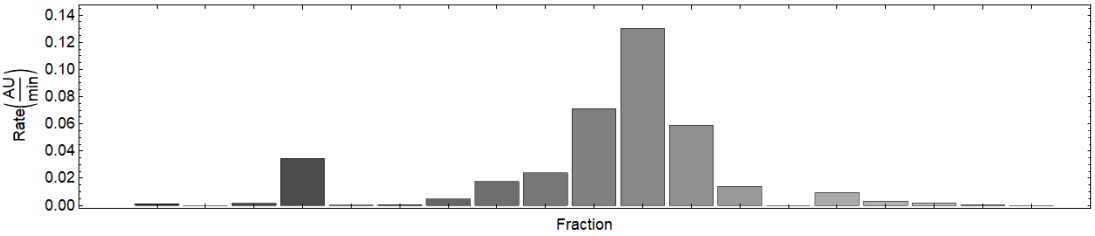

Fig. 3: Observed rate of urate decomposition (AU/min) of each 2.0 mL Ni-NTA fraction.

3.4 SDS Polyacrylamide Gel Electrophoresis

All lanes displaying visible signals are shown in Fig. 4 below. The only chromatography fractions that displayed visible signal were Fractions 1-2.

Fig. 4: Samples loaded in each lane of the SDS-PAGE gel. All samples were mixed 2:1 (v%) sample:4X Laemmli Sample Buffer (Bio-Rad Laboratories, Inc.) and underwent heat treatment (95 °C, 5m) in a T100™ Thermal Cycler (Bio-Rad Laboratories, Inc.) and spun at maximum speed in a microcentrifuge (USA Scientific[7]) to pellet insoluble material and loaded at a total volume of 12 μL of sample (or 7 μL of protein standard).

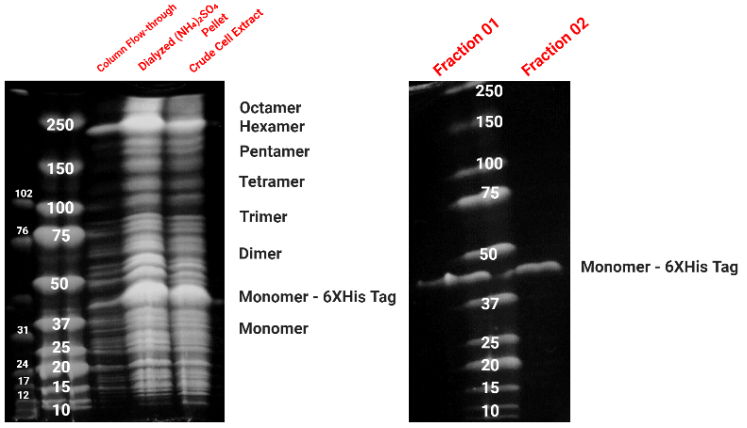

Lane	Contents
1	F # 01
2	Standard[a]
3	F # 02
4	F # 03
5	F # 04
6	F # 05
7	F # 06
8	F # 07
9	F # 08
10	F # 09
11	F # 10
12	F # 11
13	F # 12
14	F # 13
15	F # 14

Lane	Contents
16	F # 15
17	F # 16
18	F # 17
19	F # 18
20	F # 19
21	Crude Cell Lysate
22	Dialyzed $(NH_4)_2SO_4$ Pellet
23	Column Flow-Through
24	Standard[a]
25	Standard[a]
26	Standard[b]

[a] Precision Plus Protein Kaleidoscope Standards, Bio-Rad Laboratories, Inc. [b] Full-Range Rainbow Markers, GE Healthcare

4 Discussion

4.1 Cell Lysis

The activity in the crude cell lysate shows that cell lysis was successful. After nucleic acids were precipitated by addition of protamine sulfate and the nucleic acid-protamine sulfate complexes were pelleted, the activity decreased significantly. This indicates that some enzyme activity was lost due to either the protamine sulfate treatment, despite the amount of protamine sulfate added (3.0 mg) falls within the suggested range of 1.3-3.3 mg[3], or excessive sonication.
Next, ammonium sulfate was used to selectively precipitate urate oxidase. Due to a calculation error, too much was added. However, after pelleting the protein, the activity in the supernatant was negligible. This indicates that active enzyme has been pelleted and no longer remains in solution. Additionally, When redissolved in Buffer A and after dialysis against Buffer A, the specific activity increased dramatically. Thus, although it is most likely that some enzyme activity was lost initially, ammonium sulfate treatment and dialysis were successful in retaining enzymatic activity.

Tab. 2: Activity assay results throughout the process of purification of 665.3 mg of cell paste.

Step	Activity (U/mL)	Units of Enzyme (U)	Specific Activity (U/mg)	Yield (%)	Enzyme (mg)	Enzyme Yield (%)
Crude cell lysate	0.54330122	8.692819512	0.285459146	100.00	30.4520616	100.00
Precipitation with protamine sulfate	0.423380488	6.774087805	0.210500753	73.74	32.18082464	105.68
Redissolved $(NH_4)_2SO_4$ pellet	0.807142886	13.72142907	0.414881233	145.34	33.07314953	108.61
Dialyzed $(NH_4)_2SO_4$ pellet	0.817682927	2.45304878	0.397463503	139.24	6.171758569	20.27
Chromatography (pooled)	0.081300813	0.731707317	0.228493594	80.04	3.202309985	10.52
Dialysis	0.076219512	0.266768293	0.279942341	98.07	0.952940136	3.13
Concentrated (Final preparation)	2.662601626	0.266260163	14.10836734	4942.34	0.0188725	0.06

4.2 Nickel Affinity Column Chromatography

The issues with the equipment described earlier and the associated significant loss of eluant is reflected in the purification table, despite pooling together the fractions with the most significant activity. Notably, for the first time in the procedure, the protein concentration drops dramatically.

4.3 SDS Polyacrylamide Gel Electrophoresis

The molecular weight of uricase was determined by sodium dodecyl sulphate-polyacrylamide gel electrophoresis (SDS-PAGE) as per the method described by Laemmli[25] to be about 35-37 kDa. Fractions 1 and 2 both display bands at molecular weight 35.0 kDa, corresponding to monomeric UOx with the expected 6X-His tag. In the lanes containing the crude cell lysate, the dialyzed ammonium sulfate pellet, and the column flow-through, the most intense bands occur around 140 kDa and 210 kDa, which reflect the weights of tetrameric and hexameric UOx. Although the sample buffer contains DTT, which should allow the subunits of multimeric proteins to migrate as monomers, it is not uncommon for reoxidation and formation of disulfide bonds within proteins to occur during electrophoresis. One could potentially minimize this phenomenon by addition of an antioxidant (such as $NaHSO_3$) to the inner running buffer before initiating electrophoresis.[22]
Although Fractions 7-12 displayed the most enzymatic activity in the activity assays, none of the fractions resulted in any visible bands upon visualization of the gel. Coomassie brilliant blue R-250 has a detection limit of 0.1–0.5 μg.[30] The average protein concentration the six pooled fractions was 0.06 mg/mL; from here, we find that only 0.48 μg of total protein, on average, would be present in Lanes 8-13 (which contain Fractions 7-12). Thus, the lack of of visible bands in these lanes may be possibly remedied by using a more sensitive staining method[4]

4.4 Concentration and Buffer Exchange

The final steps of the purification resulted in another dramatic increase in specific activity, while decreasing the sample volume to an easily managable size.
In general, in order to prevent any thermal denaturation, care was taken to keep protein fractions cold as much as possible. Additionally, because urate oxidase is unstable until it is significantly purified, we expect some loss of activity due to the prolonged timespan of the purification process.

5 Conclusion

Overall, the purification of WT urate oxidase was successful. Although a few areas of the process would absolutely benefit from self-practice, the specific activity of the enzyme generally increased throughout purification while the amount of protein decreased. Additionally, the concentrated final sample was successfully applied for kinetic measurements.

[3] 2-5 mg of protamine sulfate per gram of cell paste
[4] For example, one could potentially make use of silver staining, chemiluminesent dyes, or immunofluorescent methods[22]

Appendix I

Tab. 3: Recipes used for buffers, as instructed.[22]

Buffer	Recipe
Lysis Buffer	25 mM Tris-HCl pH 8.0, 10 mM Na_2SO_4, 1 mM phenylmethanesulfonyl fluoride (PMSF)[a], 0.5 mg/mL lysozyme, 2 mM EDTA, 0.5% Tergitol NP-10 and 0.075% polymyxin B
Buffer A	20 mM potassium phosphate, pH 7.4, 10 mM imidazole and 0.4 M NaCl
Buffer B	20 mM potassium phosphate, pH 7.4, 40 mM imidazole and 0.4 M NaCl
Buffer C	20 mM potassium phosphate, pH 7.4, 500 mM imidazole and 0.4 M NaCl
Resolving gel overlay solution	0.375 M Tris-HCl, 0.1% SDS, pH 8.8
Sample buffer	3.5 mL H_2O, 1.3 mL 0.5 M Tris, pH 6.8, 2.5 mL glycerol, 2 mL 10% SDS, 0.2 mL 0.5% bromophenol blue, 50 mM DTT
Running buffer	25 mM Tris, pH 8.3, 192 mM glycine, 0.1% SDS
Staining solution	0.025% Coomassie Blue R-250, 7% (v/v) acetic acid, 40% (v/v) methanol in H_2O
Destaining solution 1	7% (v/v) acetic acid, 40% (v/v) methanol in H_2O
Destaining solution 2	7% (v/v) acetic acid, 5% (v/v) methanol in H_2O
Gel storage solution	1% (v/v/) glycerol, 4% (v/v) acetic acid, 40% (v/v) ethanol in H_2O
Protein storage solution	50 mM Tris, pH 8.0, 2 mM DTT

[a] Added immediately prior to use.

Tab. 4: Recipes used for SDS-PAGE gels, as instructed by the manufacturer and inspired by Laemmli et. al.[25]

	12% Resolving gel	4% Stacking gel
40% Acrylamide/Bis solution[a]	3.0 mL	0.3 mL
1.5 M Tris-HCl, pH 6.8	—	0.75 mL
1.5 M Tris-HCl, pH 8.8	2.5 mL	—
10% SDS solution	0.1 mL	30 μL
Distilled deionized water (degassed)	4.4 mL	1.90 mL
N,N,N',N'-tetramethylethylenediamine, TEMED[a]	5 μL	3 μL
10% Ammonium persulfate	50 μL	15 μL

[a] Bio-Rad Laboratories, Inc.

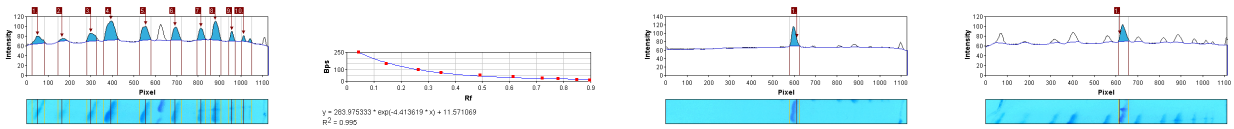

(a) Molecular weight ladder. (b) Molecular weight ladder calibration curve. (c) Fraction #1 (d) Fraction #2

Fig. 5: Screen captures of GelAnalyzer analysis of the Gel containing Lanes 1 through 15.

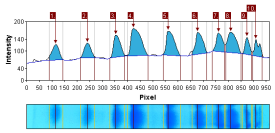

(a) Molecular weight ladder #01

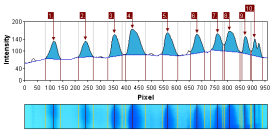

(b) Molecular weight ladder #02

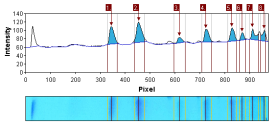

(c) Molecular weight ladder #03

(d) Calibration curve

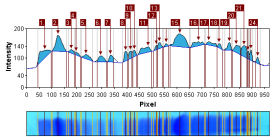

(e) Crude cell extract

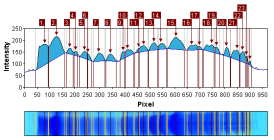

(f) Dialyzed $(NH_4)_2SO_4$ pellet

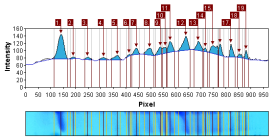

(g) Column flowthrough

Fig. 6: Screen captures of GelAnalyzer analysis of the Gel containing Lanes 16 through 30.

Tab. 5: Estimates of total protein concentration in the crude cell lysate based on A_{260} and A_{280} values.

Sample:Buffer (*v*/*v*)	A_{280}	A_{260}	A_{260}/A_{280}	[Total Protein] (mg/mL)		
				Measured	Total[a]	True[b]
1:19	0.9911	1.8826	1.90	0.11	2.00	1.60
1:39	0.4653	0.8913	1.92	0.04	1.71	1.31
1:79	0.1030	0.1920	1.86	0.01	1.08	0.68

[a] Accounts for the dilution of the sample. [b] Accounts for the presence of 0.4 mg/mL lysozyme in the sample.

Tab. 6: Bradford Assay BSA Standards.

[BSA] (mg/mL)	A_{BSA}
1.21	0.960
1.00	0.825
0.80	0.705
0.60	0.497
0.40	0.322
0.20	0.202
0.00	0.000

Fig. 7: Bradford Assay BSA Standards.

	Estimate	Standard Error	t-Statistic	P-Value	Confidence Interval
M	0.800632	0.0267463	29.9343	7.80326×10^{-7}	(0.731879, 0.869386)
B	0.0200483	0.0193508	1.03605	0.347663	(-0.0296944, 0.069791)

Additional Questions

1. **In this course you used horseradish peroxidase-based immunodetection in the dot-blot format. In principle, this methodology can be extended for the detection of coronavirus in the respiratory droplets of an infected person. Write a concise (no more than 1 page) essay outlining challenges that one expects to face when attempting to use immunodetection for the early and non-invasive identification of coronavirus-infected persons. Propose one way to overcome the most significant challenge that you have identified. Describe the key materials that one would need to implement this idea.**

   The majority of diagnostic testing for SARS-CoV-2 (severe acute respiratory syndrome coronavirus 2) is done via real-time RT-PCR (for example, QIAstat-Dx Respiratory 2019-nCoV Panel[31]) and next-generation viral sequencing of throat swabs, sputum, stool or blood samples. However, this requires specialized facilities and is extremely costly. Tests may be denied to patients that do not display symptoms, but are, in fact, carriers. Thus, the current top priority of the World Health Organization is the creation of a simpler diagnostic test.[32]

   Sputum is a noninvasive lower respiratory tract specimen, but low amounts of 2019-nCoV patients could produce sputum for diagnostic evaluation.[33] 2019-nCoV has been shown to grow better in primary human airway epithelial cells than in standard tissue-culture cells,[34] in contrast to SARS- and MERS-CoV, which infect intrapulmonary epithelial cells more than cells of the upper airways.[35,36] A saliva sample-based diagnostic would avoid patient discomfort,[37] allow for patients to collect their own samples, reducing the risk of COVID-19 transmission and time and cost associated with specimen collection.[38]

   Immunoassays in the dot-blot format would provide a highly specific, sensitive, and rapid method to assay large amounts of samples simultaneously for the presence of viral antigens. Because such an assay does not require viral culture, it would bypass the need for special facilities, further decreasing the time and cost of testing.[39] However, no kits based on either viral antigen or serum antibodies are available.[40] Antibody-based diagnostics are generally less sensitive than nucleic acid-based tests, and because they are meant to detect the body's immune response to a pathogen, which takes time to develop, these tests may not detect early stages of the illness.

   While viral proteins are, in this case, a preferable diagnostic target, multiple reports show that the genome of SARS-CoV-2 is 75 to 80% identical to that of the SARS-CoV and even more closely related to several bat coronaviruses.[41] Additionally, coronaviruses have error-prone RNA-dependent RNA polymerases, which results in a higher frequency of mutation and recombination events,[34] increasing the likelihood that the virus will be able to escape detection.

   Although monoclonal antibodies provide the highest level of specificity, they are time-consuming and laborious to prepare, especially in large batches. However, immunogenic peptides that recognize multiple epitopes have successfully been designed for the diagnosis of other pathogens.[42] In fact, several epitopes within the spike glycoprotein of SARS-COV-2 have been identified for the production of an immunogenic vaccine.[43]

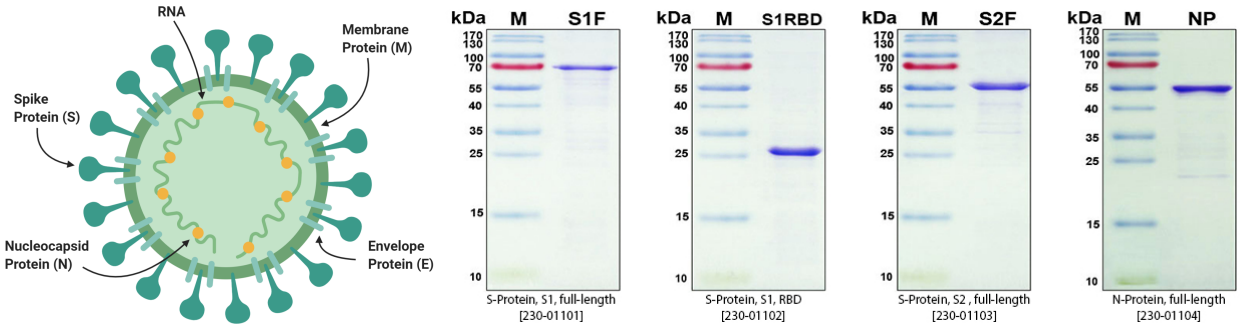

Fig. 8: General structure and components of COVID-19 (left); SDS-PAGE analysis of the purified recombinant SARS-CoV-2 target proteins (right).[44]

Parameter	Culture-Based Assays		Immunology-Based Assays		Molecular, Nucleic Acid Amplication Assays
	Viral Culture	Shell Vial	Antibody Detection	Rapid Antigen Detection	
Turnaround time	Slow (2-14d)	Moderate (2-3d)	Rapid (1d)	Very rapid (sec.-min.)	Rapid (min.-hr.)
Target	Changes in cell morphology (cytopathic effect)	Viral proteins produced after replication in cells	Host antibodies	Viral Proteins	Nucleic acid
Labor	High	Moderate	Low (if automated) or moderate (if manual)	Low	Low (newer assays) or moderate (older assays)
Sensitivity	Poor-Moderate	Moderate	Variable (immuno-supressed persons may not mount adequate antibody responses)	Poor (Exception: HIV testing)	High
Specificity	Low (cytopathic effects between viruses can overlap)	Moderate - Monoclonal antibodies impart specificity but may cross-react with other proteins. - Interpretation can be subjective.	Moderate (Crossreactive antibodies can decrease specificity)	Variable	High
Breadth	Moderate (5-10 viruses)	Limited (1 per vial)	Limited (some cross-reactive antibodies can detect closely related viruses)	Limited	Extensive (Newer assays detect >20 targets) or limited (Older assays detect 1-3 targets)
Specimen type	Many	Many	Blood components or CSF	Varies	Limited (Different specimen types must be validated separately)
Cost of reagents	Low	Moderate	Low-Moderate	Low	High
Risk of infection	Moderate (Other viruses may grow unexpectedly.)	Low-Moderate	Low	Low	Low

Tab. 7: Types of assays used in diagnostics of viral infections.[45]

References

[1] Jessica Hochberg and Mitchell S. Cairo. Tumor lysis syndrome: Current perspective. *Haematologica*, 93:9–13, 2008.

[2] Robert Wortmann. Recent advances in the management of gout and hyperuricemia. *Current Opinion in Rheumatology*, 17(3):319–324, 2005.

[3] L. K. Stamp, J. L. O'Donnell, and P. T. Chapman. Emerging therapies in the long-term management of hyperuricaemia and gout. *Internal Medicine Journal*, 37(4):258–266, 2007.

[4] Tariq I. Mughal, A. Ahsan Ejaz, John R.Foringer, and Bertrand Coiffier. An integrated clinical approach for the identification, prevention, and treatment of tumor lysis syndrome. *Cancer Treatment Reviews*, 36(2):164–176, 2010.

[5] Sanofi-Aventis. Elitek (rasburicase) for injection for intravenous use [prescribing information]. *Bridgewater, NJ*, 2017.

[6] Stanton C. Goldman, John S. Holcenberg, Jerry Z. Finklestein, Raymond Hutchinson, Susan Kreissman, F. Leonard Johnson, Conrad Tou, Elizabeth Harvey, Erin Morris, and Mitchell S. Cairo. A randomized comparison between rasburicase and allopurinol in children with lymphoma or leukemia at high risk for tumor lysis. *Blood*, 97(10):2998–3003, 2001.

[7] Kalju Kahn and Peter A. Tipton. Kinetic mechanism and cofactor content of soybean root nodule urate oxidase. *Biochemistry*, 36(16):4731–4738, 1997.

[8] Anjana V. Yeldandi, Vijay Yeldandi, Sujata Kumar, C. V. Narasimha Murthy, Xuedong Wang, Keith Alvares, M. Sambasiva Rao, and Janardan K. Reddy. Molecular evolution of the urate oxidase-encoding gene in hominoid primates: nonsense mutations. *Gene*, 109(2):281–284, 1991.

[9] Nathalie Colloc'h, Mohamed El Hajji, Bernard Bachet, Guillaume L'Hermite, Marc Schiltz, Thierry Prangé, Bertrand Castro, and Jean-Paul Mornon. Crystal structure of the protein drug urate oxidase-inhibitor complex at 2.05 Å resolution. *Nature Structural Biology*, 4:947–952, 1997.

[10] Nathalie Colloc'h, Anne Poupon, and Jean-Paul Mornon. Sequence and structural features of the t-fold, an original tunnelling building unit. *Proteins*, 39(2):142–154, 2000.

[11] MS Cairo, S Thompson, K Tangirala, and MT Eaddy. A clinical and economic comparison of rasburicase and allopurinol in the treatment of patients with clinical or laboratory tumor lysis syndrome. *Clin Lymphoma Myeloma Leuk*, 17(3):173, 2017.

[12] X Feng, K Dong, D Pham, S Pence, J Inciardi, and NS Bhutada. Efficacy and cost of single-dose rasburicase in prevention and treatment of adult tumour lysis syndrome: a meta-analysis. *J Clin Pharm Ther*, 38(4):301–308, 2013.

[13] G Sibony, M L North, J P Bergerat, J M Lang, and F Oberling. Hyperuricemia resistant to urate oxidase. role of anti-serum urate oxidase precipitating antibodies. *Presse medicale*, 13(7), 1984.

[14] Maureen Deehan, Sandra Garcês, Daniel Kramer, Matthew P. Baker, Dorothea Rat, Yvonne Roettger, and Arno Kromminga. Managing unwanted immunogenicity of biologicals. *Autoimmunity Reviews*, 14(7):569–574, 2015.

[15] Eric Girard, Stéphane Marchal, Javier Perez, Stéphanie Finet, Richard Kahn, Roger Fourme, Guillaume Marassio, Anne-Claire Dhaussy, Thierry Prangé, Marion Giffard, Fabienne Dulin, Françoise Bonneté, Reinhard Lange, Jacques H. Abraini, Mohamed Mezouar, , and Nathalie Colloc'h. Structure-function perturbation and dissociation of tetrameric urate oxidase by high hydrostatic pressure. *Biophys J*, 98(10):2365–2373, 2010.

[16] Michael S. Caves, Barry K. Derham, Jan Jezek, and Robert B. Freedman. Thermal inactivation of uricase (urate oxidase): Mechanism and effects of additives. *Biochemistry*, 52(3):497–507, 2013.

[17] Flaviu Gruia, Arun Parupud, Manuel Baca, Chris Ward, Andrew Nyborg, Jr. Richard L. Remmele, and Jared S. Bee. Impact of mutations on the higher order structure and activity of a recombinant uricase. *Journal of Pharmaceutical Sciences*, 106(4):1018–1024, 2017.

[18] T. G. Conley and D. G. Priest. Thermodynamics and stoicheiometry of the binding of substrate analogues to uricase. *Biochemical Journal*, 187(3):727–732, 1980.

[19] Yi Shi, Wang Ting, Edward X. Zhou, Qiu feng Liu, Yi Jiang, and Eric H. Xu. Designing a mutant candida uricase with improved polymerization state and enzymatic activity. *Acta Pharmacologica Sinica*, 40(10):1364–1372, 2019.

[20] Lei Tao, Dandan Li, Yonghong Li, Xinchang Shi, Junzhi Wang, Chunming Rao, and Yingqi Zhang. Designing a mutant candida uricase with improved polymerization state and enzymatic activity. *Protein Engineering, Design & Selection*, 30(11):753–759, 2017.

[21] *Protocol for Protein Expression Using BL21 (C2530)*. New England Biolabs, Inc., https://www.neb.com/protocols/0001/01/01/protocol-for-protein-expression-using-bl21-c2530, 2020.

[22] Kalju Kahn. *The Operations Manual for Component 2: 'Urate Oxidase'*. University of California, Santa Barbara, Santa Barbara, CA, 2019.

[23] Paul T. Wingfield. Protein precipitation using ammonium sulfate. *Curr Protoc Protein Sci.*, 13(1):A3F1–A3F8, 1998.

[24] Inc. Bio-Rad Laboratories. Mini-protean® tetra cell instruction manual.

[25] U. K. Laemmli. Cleavage of structural proteins during the assembly of the head of bacteriophage t4. *Nature*, 227:680–685, 1970.

[26] Kalju Kahn, Stanley Parsons, and Jonathan Kohn. *Theory Manual: Laboratory Techniques in Biochemistry*. University of California, Santa Barbara, Santa Barbara, CA, 2019.

[27] Kalju Kahn and Peter A. Tipton. Spectroscopic characterization of intermediates in the urate oxidase reaction. *Biochemistry*, 37(33):11651–11659, 1998.

[28] Kalju Kahn. *The Operations Manual for Component 3: 'Urate Oxidase: The Large Protein'*. University of California, Santa Barbara, Santa Barbara, CA, 2020.

[29] Bio-Rad. *Bio-Rad Protein Assay*. LIT33C.

[30] Julie L. Brunelle and Rachel Green. Chapter thirteen - coomassie blue staining. *Methods in Enzymology*, 541:161–167, 2014.

[31] QIAGEN. Qiagen announces worldwide shipments of qiastat-dx test kits for sars-cov-2., 2020.

[32] Heathcare Purchasing News. Saliva test may work as first coronavirus test., 2020.

[33] Jin-Wei Ai, Jun-Wen Chen, Yong Wang, Xiao-Yun Liu, Wu-Feng Fan, Gao-Jing Qu, Mei-Ling Zhang, Sheng-Duo Pei, Bo-Wen Tang, Shuai Yuan, Yang Li, Li-Sha Wang, Guo-Xin Huang, and Bin Pei. The cross-sectional study of hospitalized coronavirus disease 2019 patients in xiangyang, hubei province. *medRxiv*, Preprint, 2020.

[34] Stanley Perlman. Another decade, another coronavirus. *N Engl J Med*, 382(8):760–762, 2019.

[35] Peter KC Cheng, Derek A Wong, Louis KL Tong, Sin-Ming Ip, Angus CT Lo, Chi-Shan Lau, Eugene YH Yeung, and Wilina WL Lim. Viral shedding patterns of coronavirus in patients with probable severe acute respiratory syndrome. *The Lancet*, 363(9422):1699–1700, 2004.

[36] David S Hui, Esam I Azhar, Yae-Jean Kim, Ziad A Memish, Myoung don Oh, and Sir Alimuddin Zumla. Middle east respiratory syndrome coronavirus: risk factors and determinants of primary, household, and nosocomial transmission. *The Lancet: Infectious Diseases*, 18(8):e217–e227, 2018.

[37] Karin B. Hansen, Johan Westin, Lars-Magnus Andersson, Magnus Lindh, Anders Widell, and Anna C. Nilsson. Flocked nasal swab versus nasopharyngeal aspirate in adult emergency room patients: similar multiplex pcr respiratory pathogen results and patient discomfort. *Infectious Diseases*, 48(3):246–250, 2015.

[38] KKW To, CCY Yip, CYW Lai, CKH Wong, DTY Ho, PKP Pang, ACK Ng, KH Leung, RWS Poon, KH Chan, VCC Cheng, IFN Hung, and KY Yuen. Saliva as a diagnostic specimen for testing respiratory virus by a point-of-care molecular assay: a diagnostic validity study. *Clinical Microbiology and Infection*, 25(3):372–378, 2019.

[39] Fathy Gaber and Sanjay Kapil. Development of an antigen spot test for detection of coronavirus in bovine fecal samples. *American Society for Microbiology Journals*, 1999.

[40] Qiang Shu Ying-Hu Chen Chun-Zhen Hua Fu-Bang Li Ru Lin Lan-Fang Tang Tian-Lin Wang Wei Wang Ying-Shuo Wang Wei-Ze Xu Zi-Hao Yang Sheng Ye Tian-Ming Yuan Chen-Mei Zhang Zhi-Min Chen, Jun-Fen Fu and Yuan-Yuan Zhang. Diagnosis and treatment recommendations for pediatric respiratory infection caused by the 2019 novel coronavirus. *World Journal of Pediatrics*, 2020.

[41] Xian-Guang Wang Ben Hu Lei Zhang-Wei Zhang Hao-Rui Si Yan Zhu Bei Li Chao-Lin Huang Hui-Dong Chen Jing Chen Yun Luo-Hua Guo Ren-Di Jiang Mei-Qin Liu-Ying Chen Xu-Rui Shen Xi Wang Xiao-Shuang Zheng Kai Zhao Quan-Jiao Chen Fei Deng Lin-Lin Liu Bing Yan Fa-Xian Zhan Yan-Yi Wang Gengfu Xiao Zheng-Li Shi Peng Zhou, Xing-Lou Yang. Discovery of a novel coronavirus associated with the recent pneumonia outbreak in humans and its potential bat origin. *Nature*, 79(104212), 2020.

[42] Xiuling Song-Han Li Juan Wang Wen Ju-Xiaofeng Qu Dandan Song Yushen Liu Xiangjun Meng Hongqian Cao-Weiyi Song Rizeng Meng Jinhua Liu Juan Li Dehui Yin, Li Li and Kun Xu. A novel multi-epitope recombined protein for diagnosis of human brucellosis. *BMC Infectious Diseases*, 16(219), 2016.

[43] Manojit Bhattacharya, Ashish R. Sharma, Prasanta Patra, Pratik Ghosh, Garima Sharma, Bidhan C. Patra, Sang-Soo Lee, and Chiranjib Chakraborty. Development of epitope-based peptide vaccine against novel coronavirus 2019 (sars-cov-2): Immunoinformatics approach. *Journal of Medical Virology*, 44, 2020.

[44] Inc. RayBiotech. Covid-19 proteins.

[45] Reeti Khare. *Guide to Clinical and Diagnostic Virology*. John Wiley & Sons, 2019.